



**HAL**  
open science

## Ultraviolet vs. Visible Skylight Polarization Measurements

Antoine Moutenet, Julien Serres, Stéphane Viollet

► **To cite this version:**

Antoine Moutenet, Julien Serres, Stéphane Viollet. Ultraviolet vs. Visible Skylight Polarization Measurements. IEEE Sensors 2023, IEEE, Oct 2023, Vienna, Austria. 10.1109/SENSORS56945.2023.10325144 . hal-04267719

**HAL Id: hal-04267719**

**<https://hal.science/hal-04267719v1>**

Submitted on 2 Nov 2023

**HAL** is a multi-disciplinary open access archive for the deposit and dissemination of scientific research documents, whether they are published or not. The documents may come from teaching and research institutions in France or abroad, or from public or private research centers.

L'archive ouverte pluridisciplinaire **HAL**, est destinée au dépôt et à la diffusion de documents scientifiques de niveau recherche, publiés ou non, émanant des établissements d'enseignement et de recherche français ou étrangers, des laboratoires publics ou privés.



Distributed under a Creative Commons Attribution 4.0 International License


# Ultraviolet vs. Visible Skylight Polarization Measurements

Antoine Moutenet 

Safran Electronics&Defense  
Massy, France

Aix Marseille Univ, CNRS, ISM  
Marseille, France

Email: antoine.moutenet@univ-amu.fr

Julien R. Serres 

Institut Universitaire de France (IUF)  
Paris, France

Aix Marseille Univ, CNRS, ISM,  
Marseille, France

Email: julien.serres@univ-amu.fr

Stéphane Viollet 

Aix Marseille Univ, CNRS, ISM  
Marseille, France

Email: stephane.viollet@univ-amu.fr

**Abstract**—Concerning autonomous navigation in GNSS-denied environments, insects like bees, ants, locusts and butterflies are certainly the cup winners. Bees and some ants are known to be sensitive to polarized light, both in ultraviolet (UV) and visible spectra, and to use it for their outside moving heading calculation. Therefore, we chose to compare UV and visible skylight polarization measurements in order to understand how UV could be used to improve heading estimation by processing the skylight’s angle of polarization patterns. We then used a commercial polarimetric camera sensitive to visible polarized light and a UV-sensitive camera enhanced with polarized light measurement ability.

**Index Terms**—Ultraviolet (UV), skylight polarization, Rayleigh scattering, celestial compass, polarized vision.

## I. INTRODUCTION

Autonomous outdoor navigation is mainly based on Global Navigation Satellite Systems (GNSS), magnetic compass and gyro-compass but it requires redundant, robust and affordable strategies to be reliable in all conditions (weather, electromagnetic disturbances...). A nowadays scope is bio-inspired compass based on the measurement of the skylight polarization patterns, which have been found efficient in GNSS or magnetic compass denied environments [1].

Those sensors are basically sun-finder devices relying on polarization, coupled with ephemerides computation in order to find true North. Indeed visible and near visible skylight should be scattered such as polarization direction is always perpendicular to sun-observer direction according to Rayleigh scattering theory.

Although most of those polarimetric sensors are only focusing on visible spectrum, which, still according to Rayleigh scattering theory, is supposed to be more reliable than UV, insects like ants and bees curiously use polarization in both spectra for their outside moving heading calculation [2].

To investigate how UV could be used to improve heading by skylight polarization, we chose as our peers [3]–[7] to compare UV and visible skylight polarization measurements.

A.M. was supported by a CIFRE doctoral fellowship from the ANRT and Safran Electronics & Defense (agreement #2021/0056). J.R.S has received funding from the Excellence Initiative of Aix-Marseille Université - A\*Midex, a French “Investissements d’Avenir” programme AMX-21-ERC-02 and AMX-20-TRA-043. This research work was also supported by the SUD Provence-Alpes-Côte d’Azur Region (PACA) (Grant #2021/08135).

In our study, we will focus on sun finding, especially sun-azimuth finding and compare the UV response with the visible response to select the most worthy to be used, depending on sky conditions.

## II. OBSERVED POLARIZATION PHENOMENON

Polarization effect of single elastic scattering for particles much smaller than wavelength (Rayleigh scattering) could be simplified as follows: each charged particle acts like an antenna moving in the incident electrical field perturbation plane, and each observer around this far particle sees differentially the electrical field perturbation generated by it regarding his own position, which generates linear partial polarization (Fig. 1).

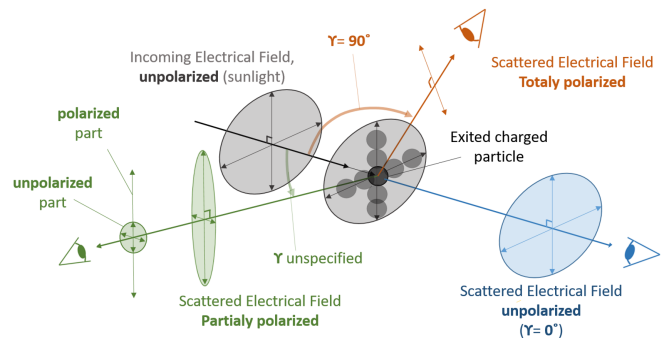


Fig. 1. Skylight single scattering and polarization.  $\gamma$  is the scattering angle.

The degree of linear polarization ( $DoLP$ ) and the angle of polarization ( $AoP$ ) of an observed point or coming ray are then defined as the ratio between polarized light intensity and total light intensity, and the angle between polarization orientation and a reference axis, respectively.

If we decompose the scattered electric field in parallel and orthogonal components to the scattering plane, than there corresponding intensities and  $DoLP$  can be express as (1), with  $\gamma$  the scattering angle. The  $AoP$  expression will change depending on the chosen reference axis, but the key property is that polarization orientation is perpendicular to the scattering plane.

We chose to name  $AoP_l$  for the *local* angle of polarization, which means the angle between polarization orientation and

the sky meridian plane of scattered light, so  $AoP_l$  depends on the observed direction.

Sun azimuth is the azimuth of the meridian verifying  $AoP_l$  equal to  $\pm 90^\circ$ .

$$DoLP = \frac{I_{scatt_{ortho}} - I_{scatt_{para}}}{I_{scatt_{ortho}} + I_{scatt_{para}}} = \frac{1 - \cos(\gamma)^2}{1 + \cos(\gamma)^2} \quad (1)$$

This single scattering model is reliable only for near visible spectrum in clear sky conditions. With clouds and aerosols, multiple scattering and Mie scattering occur, leading to changes in  $AoP$  distribution and to the appearance of four neutrals points (null  $DoLP$ ) instead of two neutral points [8], [9]. The only two remaining polarization parameters are the symmetry regarding to the solar meridian (for homogeneous skies) and that the solar meridian is still characterized by a segment where  $AoP_l = 90^\circ$ .

### III. EXPERIMENTAL SETUP

Our experiment consisted in sky polarization observations, both in UV and visible spectra, for various cloud cover conditions. We used two cameras:

- The first one was a polarized monochromatic camera (FLIR Blackfly S BFS-U3-51S5P). This camera model has an add-on micro-polarizers array such as, for each square block of four pixels, the four micro-polarizers orientations are at  $0, 45, 90$  and  $135^\circ$  from the sensor length, see Fig. 2(a). This configuration allows users to easily compute Stokes parameters by differences between neighbor pixels intensities. We mounted an objective of focal length equal to 8mm, which means this camera's half-field of view was approximately  $26^\circ$ .
- The second one was a UV-sensitive camera (JAI Go-8105M-PGE-UV). As shown in Fig. 2(b), as an objective, we mounted directly onto this camera a UV-centered band-pass filter (Thorlabs FGUV5) and a pinhole ( $50\mu\text{m}$  or  $200\mu\text{m}$ ). Due to the pinhole position, this camera's half-field of view of approximately  $15^\circ$ . Above this elementary UV objective we connected a manually continuous rotating mount (Thorlabs CLR1,  $1^\circ$  precision) with UV polarizer inside (Thorlabs LPUV100), in order to be able to take images of linear polarization orientations at  $0, 45, 90$  and  $135^\circ$  from the sensor length, just like the first camera.

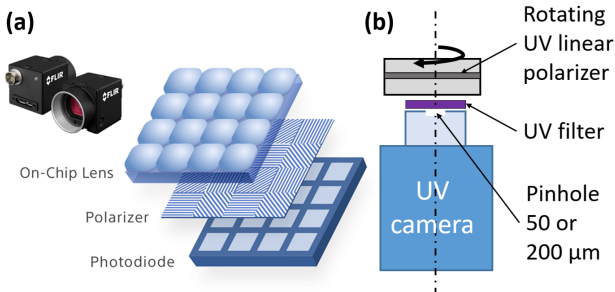


Fig. 2. (a) Visible spectrum polarized camera. Adapted from <https://www.flir.fr> and <https://www.sony-semicon.com>. (b) UV-sensitive camera fitted with a low-cost objective.

As shown in Fig. 3, the two cameras were fixed on a support rail (SR), separated from 8 centimeters of each other with their field of view aligned. The two cameras share the same image reference frame. The SR was also fixed onto a motorized rotating stage (Thorlabs PRMTZ8/M).

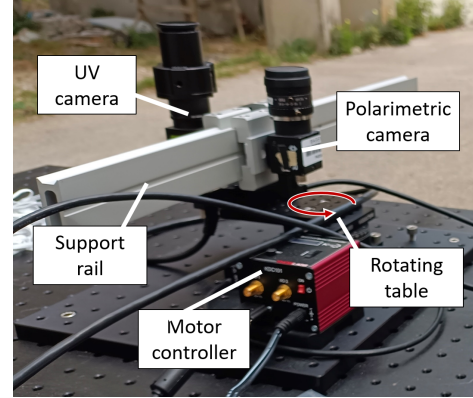


Fig. 3. Outdoor experiment. Luminy University Campus, Marseille.

Measurements were made at Marseille in France, June 2023, with clear sky, partially cloudy sky, and sky with a thin and thick blanket of clouds. For each measurement, we oriented the SR according to three positions:  $0, 10$  and  $50^\circ$  from the rotating table origin.

For each orientation, we took one image with the polarized camera, with an acquisition time of less than 0.1s and four images with the UV camera.

The set of images from the UV-sensitive camera were taken by rotating the linear polarizer in the following order:  $0^\circ, 90^\circ, 135^\circ, 45^\circ$ . The acquisition time was 8s for the  $50\mu\text{m}$  pinhole and 2s for the  $200\mu\text{m}$  pinhole. The time interval between each images was between 3 and 5s.

We implemented image processing on two separated codes: a first one which displays  $AoP_l$  and  $DoLP$  and a second one, Sun Azimuth Axis Finder, SAAF, which finds sun azimuth relying on the  $\pm 90^\circ$   $AoP_l$  property of the sun meridian. This second image processing software, inspired by H. Lu et al. [10], consists on a binary threshold on the  $AoP_l$  around  $\pm 90^\circ$  followed by a Hough transform, centered on the image's center and considering only small radius.

We calibrated rotating UV polarizer zero position by putting above our setup a fixed polarizing filter P100 Non UV-cut (from <https://3dlens.com/>) and measuring its blocking axis orientation using SAAF with the two cameras. The angular difference between the two measurements of the blocking axis was used as the  $0^\circ$  polarizer position.

### IV. RESULTS

Both images taken by the UV and polarimetric cameras were processed with same algorithms, made for polarimetric camera captures. To do so, we create polarimetric images with UV camera captures by merging images of polarization intensity at  $0^\circ, 90^\circ, 45^\circ$  and  $135^\circ$  in one single image, polarimetric camera like.

To compute  $DoLP$  and  $AoP_l$  (see Fig. 4 for examples), we use normalized Stokes parameters  $s_1$  and  $s_2$  as explained in (2).  $\alpha_p$  is the azimuth coordinate of each pixel in the image frame,  $i$  is the imaginary number. The image frame origin is the image center.

$$\begin{aligned} s_1 &= (I_0 - I_{90}) / (I_0 + I_{90}), \\ s_2 &= (I_{45} - I_{135}) / (I_{45} + I_{135}) \\ DoLP &= \sqrt{s_1^2 + s_2^2} \\ AoP_l &= -\alpha_p + 0.5 \cdot \angle(s_1 + i \cdot s_2) \end{aligned} \quad (2)$$

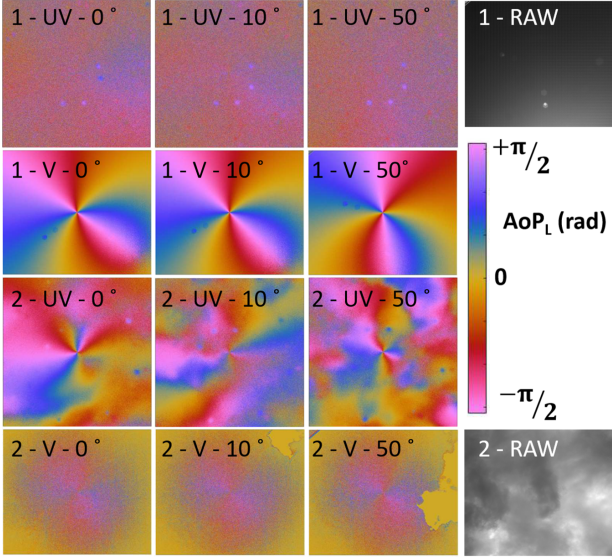


Fig. 4. Examples of  $AoP_l$  patterns computed from real images. 1 & 2 refer to two sky conditions, clear & thick cloud blanket respectively. UV is for  $AoP_l$  in the UV, V for  $AoP_l$  in the visible spectrum.  $0^\circ$ ,  $10^\circ$ ,  $50^\circ$  correspond to the angular position of the support rail. RAW is a monochromatic image of the sky.

Due to the long acquisition time of the UV camera and rotation time of the UV polarizer, the skylight intensity distribution could change from one capture to another during measurements. We call this phenomenon “sky drift”. In order to easily know how this sky drift could affect measurements on UV camera, for each experiment (3 SR angular positions), we captured 4 images with the UV camera, with a fixed polarizer position. Then, we merged them like the classical captures and use them to compute a fake  $DoLP$ . With this method, since those 4 images should be identical, we should observe a null fake  $DoLP$  all over the sky, high fake  $DoLP$  area would indicate where sky drift most disturb measurements. In our data, we classified the intensities of the sky drift as follows : *null*, *low*, *medium*, *strong* and *very strong* (eg. Fig. 5).

The order of the polarizer orientations during measurements and Stokes normalized parameters’ calculation (2) were chosen to decrease the effect of the sky drift.

Since cameras share the same image reference frame, we choose two ways to compare the visible spectrum and UV polarization measurements of the sun azimuth axis: check whether the measurements between UV and visible spectra correspond to each other and check, in each spectral band,

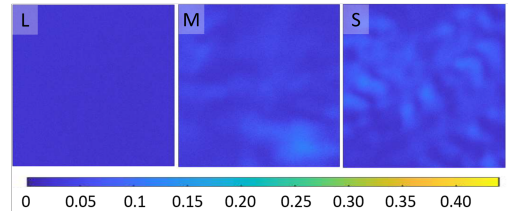


Fig. 5. Fake  $DoLP$  examples for sky drift estimation. L is a *low* sky drift, M a *medium* sky drift, S is a *strong* sky drift.

if the angular difference between azimuth measurements does correspond to the step of the SR’s rotations (see Fig. 6).

sky	measured sun azimuth axis ( $^\circ$ )			sky drift	azimuth step consistency
	SR at 0 deg	SR at 10 deg	SR at 50 deg		
clear	32.07	37.2	79.19	low	✓
	35.17	44.2	82.48	-	✓
few clouds	43.15	-2.7	47.06	strong	✗
	63.36	71.81	-68.7	-	✓
clouds	37.93	35.52	22.7	low	✗
	38.2	45.07	48.86	-	✗
big clouds	78.71	-43.33	-37.42	strong	✗
	-89.46	-1.12	0.07	-	✗
thin cloud blanket	17.2	24.56	31.04	medium	✗
thick cloud blanket	32.76	40.57	79.91	-	✓
thin cloud blanket	16.92	18.15	16.04	null	✗
thick cloud blanket	32.91	34.22	48.31	-	✗
thick cloud blanket	-4.77	-6.31	41.18	strong	~
thick cloud blanket	47.32	51.04	42.47	-	✗

Fig. 6. Sun azimuth estimation examples for various skies. Each sky condition corresponds to one experiment. Each experiment is separated in 3 angular positions of the support rail from the rotating table’s origin. The measured sun azimuth axis orientation in UV (shaded boxes) and in the visible spectrum (clear boxes) is relative to the image’s reference frame, it takes value between  $-90^\circ$  and  $+90^\circ$ . Sky drift refers to changes in skylight intensity distribution during four captures of the UV camera. Azimuth step consistency refers to correspondence between azimuth measurement and stage rotation steps.

Since the sun moved during the experiment, we should expect around  $9^\circ$  and  $39^\circ$  steps in azimuth measurements, instead of  $10^\circ$  and  $40^\circ$ . In Fig. 6 the first double row (clear) corresponds to measurement 1 in Fig. 4 and L in Fig. 5, seventh double row (thick cloud blanket) corresponds to measurement 2 in Fig. 4 and S in Fig. 5, and the fifth double row (thin cloud blanket) corresponds to M in Fig. 5.

## V. CONCLUSION

As expected from studies carried out in insects, the use of a UV-sensitive camera enhanced with polarized light measurement ability has shown that it becomes possible to estimate the sun azimuth in an overcast day. Nevertheless, this study requires further experiments by mounting a genuine objective mounted on the UV-camera (and not only a pinhole) to achieve a fair comparison with the polarimetric camera sensitive to the visible spectrum. The use of UV objective lenses will allow us to reduce drastically the acquisition time of the camera, in order to improve the accuracy of the sun azimuth estimator.

## REFERENCES

- [1] F. Kong, Y. Guo, J. Zhang, X. Fan, X. Guo, "Review on bio-inspired polarized skylight navigation," Chinese Journal of Aeronautics, May 2023.
- [2] G. Horváth and D. Varjú, "Polarized Light in Animal Vision," 2004.
- [3] X. Wang, J. Gao and Z. Fan, "Empirical corroboration of an earlier theoretical resolution to the UV paradox of insect polarized skylight orientation," Naturwissenschaften, 2014.
- [4] I. Pomozi, G. Horváth, and R. Wehner, "How the clear-sky angle of polarization pattern continues underneath clouds : full-sky measurements and implications for animal orientation," Journal of Experimental Biology, 2001.
- [5] M. Blumthaler and M. Schwarzmann, "Spectral measurements of the polarization of UV sky radiance," SPIE, 2005.
- [6] N. Carey, and W. Sturzl, "An insect-inspired omnidirectional vision system including UV-sensitivity and polarisation," IEEE International Conference on Computer Vision Workshops, 2011.
- [7] H. Zhao, W. Xu, "A Bionic Polarization Navigation Sensor and Its Calibration Method," Sensors , Vol. 16, No. 8, August 2016.
- [8] M. V. Berry, M. R. Dennis, and R. L. Jr Lee, "Polarization singularities in the clear sky," New Journal of Physics, 2004.
- [9] G. Horvath, B. Bernath, B. Suhai, and A. Barta, "First observation of the fourth neutral polarization point in the atmosphere," JOSA, 2002.
- [10] H. Lu 1, Y. Xie, K. Zhang, H. Zhang, X. M. Zou, J. Wang, and K. C. Zhao, "Construction and test of bio-inspired imaging polarization navigation prototype," The International Archives of the Photogrammetry, Remote Sensing and Spatial Information Sciences, August 2020.